ChemPubSoc Europe

DOI: 10.1002/chem.201804020

CHEMISTRY A European Journal Full Paper

Semiconductors

Adjusting Aggregation Modes and Photophysical and Photovoltaic Properties of Diketopyrrolopyrrole-Based Small Molecules by Introducing B←N Bonds

Shuting Pang[+],[a] Miriam Más-Montoya[+],*[b, c] Manjun Xiao[+],[a] Chunhui Duan,*[a] Zhenfeng Wang,[a] Xi Liu,[a] René A. J. Janssen,*[b] Gang Yu,[a] Fei Huang,*[a] and Yong Cao[a]

Abstract: The packing mode of small-molecular semiconductors in thin films is an important factor that controls the performance of their optoelectronic devices. Designing and changing the packing mode by molecular engineering is challenging. Three structurally related diketopyrrolopyrrole (DPP)-based compounds were synthesized to study the effect of replacing C–C bonds by isoelectronic dipolar B←N bonds. By replacing one of the bridging C–C bonds on the peripheral fluorene units of the DPP molecules by a coordinative B←N bond and changing the B←N bond orientation, the optical absorption, fluorescence, and excited-state lifetime of the compounds can be tuned. The substitution alters the preferential aggregation of the molecules in the solid state from H-type (for C–C) to J-type (for B←N). Introducing B←N bonds thus provides a subtle way of controlling the packing mode. The photovoltaic properties of the compounds were evaluated in bulk heterojunctions with a fullerene acceptor and showed moderate performance as a consequence of suboptimal morphologies, bimolecular recombination, and triplet-state formation.

Introduction

Solution-processed organic solar cells (OSCs) are considered to be a viable option in meeting the future global energy demand if high efficiencies can be combined with fast printing production techniques.[1] Tremendous progress has led to power conversion efficiencies (PCEs) of OSCs exceeding 14% in both single- and multijunction devices.[2] This accomplishment benefitted mainly from the development of highly efficient materials by creating novel building blocks and employing elegant synthetic strategies to combine different units.[3] So far, both small molecules and polymers exhibit promising potential for photovoltaic applications.[1c,4] However, it is still highly challenging to achieve high device performance with newly developed materials, because the device performance not only depends on the functional properties of the individual molecules, but also on their packing mode in the solid state.[5] Compared to polymers, small-molecular photovoltaic materials have a few merits, such as their well-defined molecular structures, ease of purification and characterization, and high reproducibility of their synthetic procedures.[4] Particularly the well-defined molecular structure is beneficial to developing reliable structure–performance correlations.

One of the important factors that affects the performance of small-molecule OSCs is the packing mode of molecules in films, which influences the film morphology, charge transfer, and charge-transport character.[6] H- and J-aggregation are two common packing modes of conjugated small molecules in the solid state. H-aggregates form if the adjacent molecules stack predominantly in a face-to-face arrangement, and J-aggregates if the molecules stack in a head-to-tail mode.[7] The formation of such aggregates is manifested in the energies of the excited states, the lifetime of the excitons, optical absorption spectra, and emission spectra, from which one can infer the particular aggregation motif as being predominantly H-type or J-type.[8] The aggregated state of molecular semiconductors is affected by many factors, such as the inherent electronic properties, the special functional groups, and the molecular configuration.[8,9]

[a] S. Pang,[+] M. Xiao,[+] Prof. C. Duan, Z. Wang, X. Liu, Prof. G. Yu, Prof. F. Huang, Prof. Y. Cao
State Key Laboratory of Luminescent Materials and Devices
Institute of Polymer Optoelectronic Materials and Devices
South China University of Technology, Guangzhou 510640 (P. R. China)
E-mail: duanchunhui@scut.edu.cn
msfhuang@scut.edu.cn

[b] Dr. M. Más-Montoya,[+] Prof. R. A. J. Janssen
Molecular Materials and Nanosystems, Institute for Complex Molecular Systems, Eindhoven University of Technology
P.O. Box 513, 5600 MB Eindhoven (The Netherlands)
E-mail: r.a.j.janssen@tue.nl

[c] Dr. M. Más-Montoya[+]
Present address: Department of Organic Chemistry
University of Murcia, 30100 Murcia (Spain)
E-mail: miriammas@um.es

[+] These authors contributed equally to this work.

Supporting information and the ORCID identification number(s) for the author(s) of this article can be found under: https://doi.org/10.1002/chem.201804020.

For example, changing the position of alkyl chains could tune the packing of conjugated molecules in thin films between H- and J-aggregates and thereby led to distinctly different photovoltaic performance.[9] Therefore, controlling and understanding the packing mode of conjugated materials in the solid state through molecular engineering is important to improve the device performance of small-molecule OSCs and to establish structure–property relationships.

Herein, we demonstrate that the aggregated state of diketopyrrolopyrrole (DPP)-based molecules can be influenced through subtle changes in the structure of the terminal moieties, that is, by replacing the bridging covalent C–C bonds on the terminal fluorene units by polar B←N bonds and varying the orientation of the B←N bonds (Scheme 1). The DPP fragment has been widely used to design conjugated small molecules and polymers for use in OSCs and field-effect transistors, by making use of its strong optical absorption in the visible region and excellent charge-transport properties.[10] The B←N bond is isoelectronic to the C–C bond. Replacing C–C bonds by polar B←N bonds can change the electronic properties of conjugated molecules and offers additional intermolecular dipole–dipole interactions due to the anionic character of the boron atom and the cationic character of the nitrogen atom.[11] In addition, incorporating B←N bonds into a conjugated system allows for additional structural variation, due to the directional nature of the B←N bond. Therefore, introducing B←N bonds into conjugated molecules provides a new approach to modulating the electronic properties and packing modes of organic semiconductors.[12] By introducing B←N bonds to replace the bridging C–C bonds on the terminal fluorene units and changing the orientation of B←N bonds, the aggregated state of the molecules can be tuned between H-type and J-type. The different aggregated states consequently lead to distinctly different photophysical properties and device performance in bulk-heterojunction OSCs. Our work provides a new approach to control the packing modes of organic semiconductors in thin films and favors the study of structure–property relationships of small molecular photovoltaic materials.

Results and Discussion

Design and synthesis

We use B←N units in our molecular design to modulate the packing mode of molecules in the solid state. The B←N bond is a coordination bond with a dipole moment of 5.2 D.[12d,13] The dipole orientation can affect the intermolecular π–π interactions and the arrangement of adjacent molecules. We thus synthesized two B←N-containing compounds, DPPBN-o and DPPBN-i, in which the coordinative B←N bond is oriented outward or inward, respectively, relative to the thiophene-flanked DPP core. For comparison, structurally similar DPPCC without B←N bond was also synthesized.

Compounds DPPCC, DPPBN-o, and DPPBN-i were synthesized (Scheme 1) by palladium-catalyzed Suzuki cross-coupling between dibrominated DPP core **1** and the corresponding boronic pinacol ester-bearing terminal units, that is, 2-(9,9-dimethyl-9*H*-fluoren-2-yl)-4,4,5,5-tetramethyl-1,3,2-dioxaborolane (**2**), 6,6-dimethyl-3-(4,4,5,5-tetramethyl-1,3,2-dioxaborolan-2-yl)-6*H*-5λ^4,6λ^4-benzo[3,4][1,2]azaborolo[1,5-*a*]pyridine (**3**), and 6,6-dimethyl-8-(4,4,5,5-tetramethyl-1,3,2-dioxaborolan-2-yl)-6*H*-5λ^4,6λ^4-benzo[3,4][1,2]azaborolo[1,5-*a*] pyridine (**4**), respectively, which were synthesized according to previously reported procedures.[12c,14] The blue arrows in Scheme 1 represent the dipole orientations of the B←N bonds, wherein N is positively and B is negatively charged, and the dipole is from B^- to N^+. The three DPP derivatives have good solubility in common organic solvents such as dichloromethane and chloroform.

The thermal properties of the DPP derivatives were characterized by thermogravimetric analysis (TGA) and differential scanning calorimetry (DSC) measurements (Table 1). TGA (Figure 1 a) indicated that DPPBN-o and DPPBN-i have good thermal stability with decomposition temperatures corresponding

Table 1. Thermal properties of the DPP derivatives.

	T_d [°C]	ΔH_m [J g^{-1}]	ΔH_c [J g^{-1}]	T_m [°C]	T_c [°C]
DPPCC	369	38.4	−33.2	207	154
DPPBN-o	395	61.1	−35.5	285	178
DPPBN-i	405	69.5	−59.4	294	244

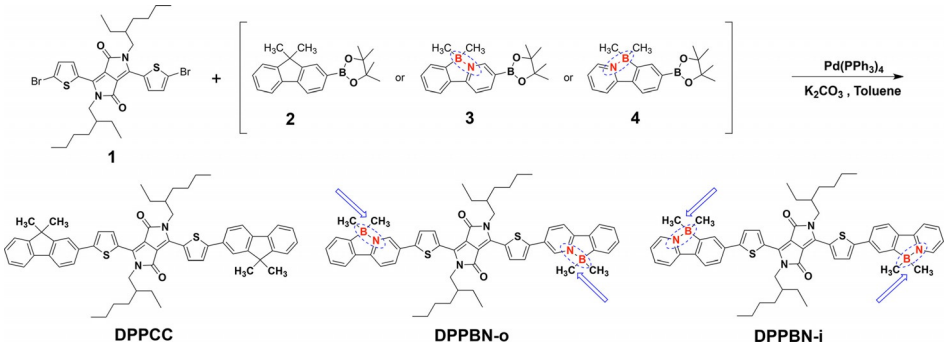

Scheme 1. Synthetic route to the DPP derivatives and structures of DPPCC, DPPBN-o, DPPBN-i bearing different terminal units. Blue arrows indicate local dipole moments.

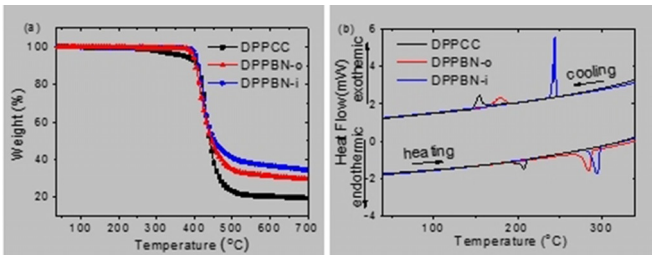

Figure 1. a) TGA and b) DSC thermograms of the DPP derivatives.

to a 5% weight loss T_d in nitrogen of 395 and 405 °C respectively, that is, higher than T_d = 369 °C of DPPCC under the same conditions. These results indicate that introducing polar B←N bonds can enhance the thermal stability. In DSC, endothermic peaks corresponding to the melting process in the second heating run were observed. Due to the presence of the polar B←N bonds, DPPBN-o (T_m = 285 °C) and DPPBN-i (T_m = 294 °C) showed much higher melting temperatures than DPPCC (T_m = 207 °C). The cooling scan featured distinct exothermic peaks corresponding to the crystallization process for DPPCC (T_c = 154 °C), DPPBN-o (T_c = 178 °C), and DPPBN-i (T_c = 244 °C) (Figure 1b). The melting enthalpy and crystallization enthalpy of DPPCC, DPPBN-o, and DPPBN-i (Table 1) also increase in the same sequence, and this suggests that the introduction of the polar B←N bonds improves the crystallinity of the conjugated compounds.

DFT calculations at the B3LYP/6-31G(d) level of theory were performed to study the geometries of the molecules. The calculations suggest that the conjugated segments of the DPP molecules with the B←N bonds maintain their coplanarity, as evidenced by the similar twist angles (Figure S1 and Table S1 in the Supporting Information).

Electrochemical properties

The electrochemical properties of the DPP compounds were studied by square-wave voltammetry (SWV) measurements on the thin films. The HOMO and LUMO energy levels were estimated from the peak positions (Figure 2).[15] Replacing the C–C bond by B←N bond shifts the HOMO and LUMO levels simultaneously downward by about 0.03–0.07 eV, consistent with the electron-withdrawing character of B←N bonds reported in the literature.[12c,d,16] The differences in the energy levels between DPPBN-o and DPPBN-i are negligible and suggest that the B←N orientation has little influence on the energy levels of the molecules. The LUMO–LUMO offsets between the DPP compounds and the electron acceptor [6,6]-phenyl-C_{61}-butyric acid methyl ester ([60]PCBM)[17] are much higher than the threshold for efficient charge dissociation (≈0.3 eV) and indicate electron-donor character of the DPP compounds relative to [60]PCBM. Moreover, all compounds have deep-lying HOMO energy levels, which are expected to give high open-circuit voltage V_{oc} in bulk-heterojunction photovoltaic devices.[18]

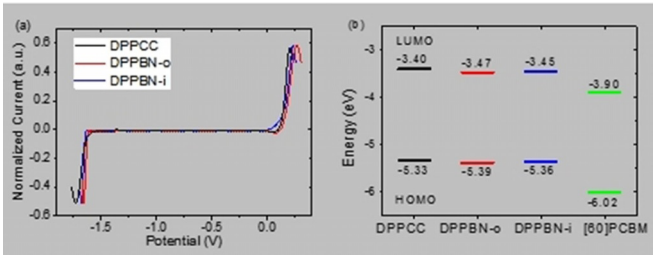

Figure 2. a) SWV measurements on the DPPs and b) energy levels of DPPCC, DPPBN-o, DPPBN-i, and [60]PCBM. A value of −5.13 eV versus vacuum for ferrocene/ferrocenium was used to determine the energy levels.[19]

Photophysical properties of DPP derivatives in solution and film

The optical properties of the DPP derivatives were evaluated by absorption and fluorescence spectroscopy in chloroform solution and as spin-coated thin films (Figure 3, Table 2). In solution, the absorption spectra of the three derivatives exhibited very similar spectroscopic features with two bands corresponding to electronic transitions with π–π* character. The intense longest-wavelength absorption bands in the range 470–700 nm are ascribed to intramolecular charge transfer. The weaker high-energy absorption bands in the 300–470 nm range can be related to localized electronic transitions of the conjugated moieties.

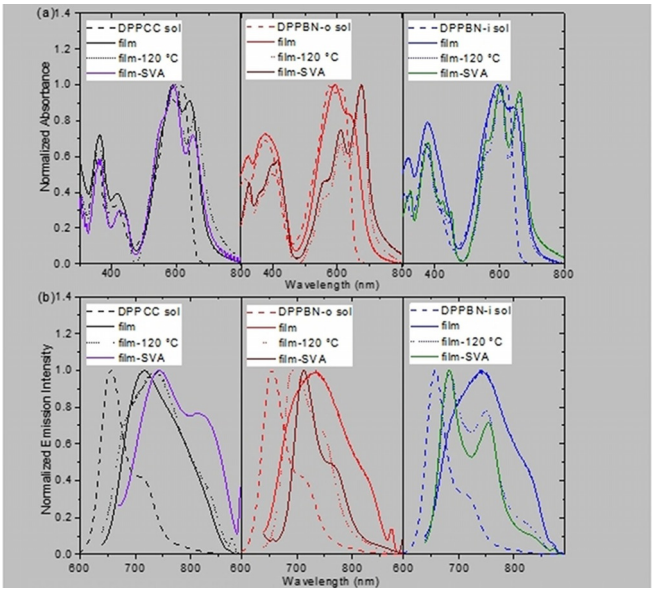

Figure 3. a) Normalized absorption and b) fluorescence spectra of the DPP derivatives in chloroform solution (dashed line), as-cast thin films (continuous line), after thermal annealing (short dash dot line), and after SVA (dotted line).

Compared to the solution spectra, a bathochromic shift is observed in the spectra of the solid thin films, characteristic of intermolecular interactions. According to Kasha's molecular exciton model, bathochromic (red) shifts of spectral bands are related to the presence of J-type aggregates in which molecules are preferentially arranged in a head-to-tail configuration.[20] Conversely, hypsochromic (blue) shifts are associated with H-

Table 2. Optoelectronic properties of DPPCC, DPPBN-o, and DPPBN-i.

Sample	Solution		Film							E_g[a] [eV]
			as-cast				solvent-annealed			
	λ_{onset} [nm]	λ_{max} [nm]	λ_{onset} [nm]	λ_{max}^{abs} [nm]	λ_{max}^{em} [nm]	$\Delta\lambda$ [nm]	λ_{max}^{abs} [nm]	λ_{max}^{em} [nm]	$\Delta\lambda$ [nm]	
DPPCC	658	618	698	641	716	75	650	743	93	1.78
DPPBN-o	660	612	706	643	734	91	675	713	38	1.76
DPPBN-i	660	619	703	644	743	99	663	685	22	1.76

[a] Estimated from the onset of the absorption spectrum of the as-cast films.

type aggregates, in which molecules stack in a face-to-face arrangement.[7a] However, this model only considers the long-range Coulombic interactions between the transition dipole moments. According to Spano's model, when the short-range interactions are also taken into account, the spectral shifts are not always representative of H-like or J-like behavior, and such aggregates can be discerned from the ratio of the first two vibronic transitions (0–0/0–1) in the absorption spectra of thin films.[21] H-aggregates exhibit a 0–0/0–1 intensity ratio smaller than unity, whereas for J-aggregates this ratio is larger than unity. In the pristine thin films of the DPP derivatives without any post-deposition treatment a 0–0/0–1 intensity ratio of less than unity was observed for the three materials, which can be interpreted as an indication of the predominant formation of H-aggregates (Figure 3a).

Post-deposition treatment is an effective method to modify the molecular packing. After post-deposition thermal or solvent-vapor annealing (SVA) of the thin films, clear differences the 0–0/0–1 peak ratios were observed between the three DPP compounds. For DPPCC, the 0–0/0–1 peak ratio became significantly less than unity and thus indicated more complete H-type aggregation. In contrast, the peak intensity ratio for DPPBN-o became distinctly larger than unity, consistent with the formation of J-aggregates on annealing. For DPPBN-i the small difference between the 0-0 and 0–1 peak intensities is tentatively attributed to aggregation intermediate between H-type and J-type.

The photoluminescence spectra of the DPPs in chloroform solution showed an intense high-energy emission band at 656–658 nm and a vibronic shoulder at longer wavelengths around 723 nm (Figure 3b). The spectral features of the fluorescence spectra of the thin films further confirmed the presence of both H-type and J-type aggregates. The photoluminescence spectra of the as-cast films (Figure 3b) show a broad and structureless band, consistent with the H-aggregation inferred from the absorption spectra. Compared with the as-cast pristine films, thermal annealing or SVA induces a redshift in the fluorescence spectra of DPPCC but a blueshift for both DPPBN-o and DPPBN-i. In particular for DPPBN-o and DPPBN-i, the spectra become narrower and clear vibronic features can be distinguished. These spectral changes are also clearly reflected in the magnitude of the (apparent) Stokes shifts $\Delta\lambda$ (Table 2), which increased for DPPCC but decreased considerably for DPPBN-o and DPPBN-i consistent with H-like and J-like aggregation, respectively.

The photoluminescence lifetimes of the thin films were measured by time-correlated single-photon counting for the pristine DPP films before and after post-deposition treatment (Table 3 and Figure S2 in Supporting Information). In general, the fluorescence lifetime traces were better fitted to biexponential decays. Theoretically, the emission from the lowest electronically excited state to the ground state is dipole-forbidden in H-aggregates and, in consequence, they have longer fluorescence lifetimes than J-aggregates, for which this radiative transition is allowed and results in shorter lifetimes. The average fluorescence lifetime of DPPCC became longer after SVA (0.65→1.79 ns), likely as a result of the more pure H-type behavior. Additionally, consistent with the J-type behavior, shorter lifetimes were measured after SVA for DPPBN-o (0.46→0.41 ns) and DPPBN-i (0.89→0.53 ns).

Table 3. Time-resolved photoluminescence parameters of the films.

Material	Treatment	A_1	τ_1 [ns]	A_2	τ_2 [ns]	τ_{avg}[a] [ns]
DPPCC	–	8.8×10^3	0.53	1.6×10^3	1.01	0.65
DPPCC	SVA	7.3×10^3	1.27	2.7×10^3	2.51	1.79
DPPBN-o	–	9.9×10^3	0.41	7.2×10^2	0.83	0.46
DPPBN-o	SVA	1.1×10^3	0.41	–	–	0.41
DPPBN-o-PCBM	–	9.1×10^3	0.60	1.0×10^3	2.07	1.00
DPPBN-o:[60]PCBM	SVA	1.1×10^3	0.37	3.8×10^2	1.24	0.84
DPPBN-i	n/a	3.9×10^3	0.53	3.5×10^2	1.97	0.89
DPPBN-i	SVA	9.9×10^3	0.40	6.3×10^2	1.19	0.53
DPPBN-i:[60]PCBM	n/a	2.2×10^3	0.84	8.3×10^3	2.15	2.03

[a] $\tau_{avg} = \sum A_i\tau_i^2 / \sum A_i\tau_i$

In summary, after thermal annealing or SVA, the three DPP compounds fall into two classes: DPPCC forms H-aggregates, whereas DPPBN-o and DPPBN-i form J-aggregates. Apparently, the molecular arrangement in the solid state can be significantly affected by small changes in the chemical structure, as well as by post-treatment of the deposited thin films.

The formation and properties of long-lived excited states were studied by near-steady-state photoinduced absorption (PIA) spectroscopy for the DPP compounds in solution (Figure 4). The PIA signal from direct excitation of the DPPs was very weak. DFT calculations suggested that the triplet energies of the DPP molecules are less than 1 eV (Table 4). Therefore, PIA experiments were carried out by using [60]PCBM as triplet sensitizer, because the intersystem-crossing quantum yield from the singlet to the triplet excited state in [60]PCBM is close to unity and its T_1 energy is about 1.5 eV.[22] Since the polarity of the solvent can affect the nature of the preferred excit-

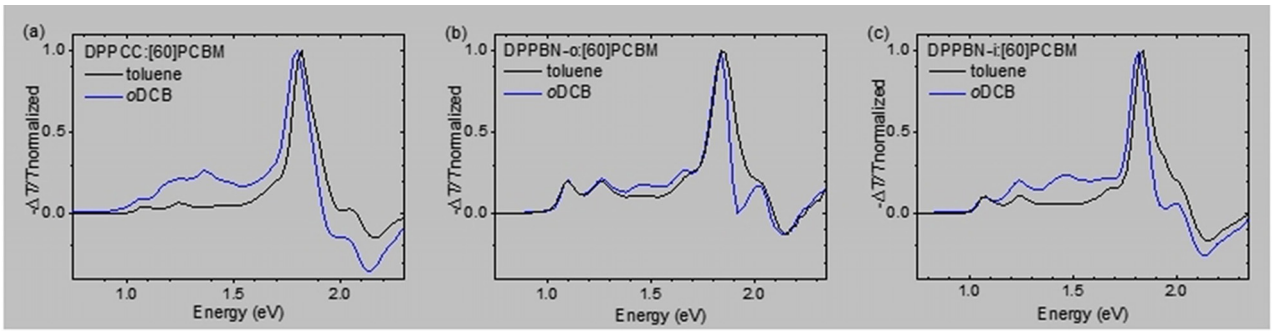

Figure 4. Normalized near-steady-state PIA spectra in toluene and *o*DCB solutions of DPP compounds (10^{-4} M) sensitized with [60]PCBM (4×10^{-4} M), recorded at room temperature, $\lambda_{exc}=364$ nm. a) DPPCC. b) DPPBN-o. c) DPPBN-i.

Table 4. Calculated singlet and triplet excited-state energies.[a]

	DPPCC	DPPBN-o	DPPBN-i
S_1 [eV]	2.20	2.18	2.18
T_1 [eV]	0.85	0.83	0.84

[a] The TDDFT calculations were performed at the ω-B97X-D/6-311G(d) level of theory.

ed states, solvents with low and high relative permittivity, that is, toluene ($\varepsilon_r=2.38$) and *ortho*-dichlorobenzene (*o*DCB, $\varepsilon_r=9.93$), were used. In media with a low relative permittivity, triplet energy transfer from the [60]PCBM T_1 state will occur. In contrast, solvents with high relative permittivity stabilize the charge-separated state and thus make electron transfer from the DPPs to the [60]PCBM T_1 state possible.

In the PIA spectra of the three DPP derivatives dissolved in toluene, recorded with excitation of [60]PCBM at 364 nm, we observed the ground-state bleaching band of the DPP compounds in the 2.0–2.5 eV range and an intense peak at 1.83 ± 0.02 eV, corresponding to $T_1\rightarrow T_n$ absorption (Figure 4). Besides, two additional and less intense PIA signals were present at lower energies (1.10 and 1.26 eV). Since charge transfer between the DPPs and [60]PCBM is not expected in toluene, these low-energy bands are ascribed to other lower-energy transitions of the triplet excited state of the DPP compounds.

The PIA spectra of the DPP compounds dissolved in *o*DCB, recorded under identical conditions, closely resemble those in toluene (Figure 4), but an additional signal at about 1.46 eV can be seen, which is tentatively ascribed to the presence of radical cations of the DPP derivatives. The characteristic spectral features of the $T_1\rightarrow T_n$ absorption of [60]PCBM, that is, a shoulder at 1.52 eV and a maximum at 1.74 eV, were not detected in the PIA spectra of the mixed solutions (Figure S3, Supporting. Information). This indicates that triplet energy transfer from the [60]PCBM T_1 state to the DPP molecules is efficient and generates the DPP molecules in their T_1 state, accompanied by some electron transfer in the more polar *o*DCB.

Photovoltaic properties

Photovoltaic properties were evaluated with an ITO/PEDOT:PSS/DPP:[60]PCBM/Ca/Al device structure under AM1.5G illumination (100 mW cm^{-2}). The photoactive layers were spin-coated from chloroform solution with a 2:1 donor:acceptor weight ratio. The device performance was fully optimized in terms of device structure, donor:acceptor ratio, thermal annealing, and SVA. Annealing with chlorobenzene (CB) vapor could significantly change the device performance of the DPP:[60]PCBM blends. The current density–voltage (*J*–*V*) characteristics of the optimized devices are shown in Figure 5a, and the photovoltaic parameters are summarized in Table 5.

As-cast films without SVA showed low short-circuit current densities J_{sc} and fill factors (FF). As a result, the devices show low overall performance with PCEs less than 1%. All devices have good V_{oc} values ranging from 0.75 to 1.01 V, consistent with their deep-lying HOMO levels. However, the variation in V_{oc} (0.25 V) is much larger than the variation in HOMO levels,

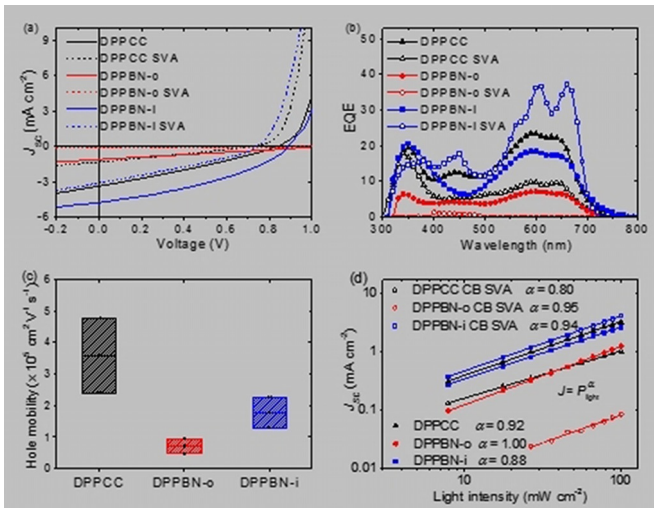

Figure 5. a) *J*–*V* characteristics of OSCs based on DPP:[60]PCBM blends under AM1.5G illumination (100 mW cm^{-2}). b) EQE spectra of the corresponding solar cells. c) Hole mobility of the DPP:[60]PCBM blended films acquired from hole-only devices with a configuration of ITO/PEDOT:PSS/DPP:[60]PCBM/MoO_3/Ag. d) Current density versus light intensity of the OSCs. ITO: indium tin oxide, PEDOT: poly(3,4-ethylenedioxythiophene), PSS: polystyrene sulfonate.

Table 5. Solar cell characteristics of the DPP:[60]PCBM OSCs under AM 1.5 G illumination (100 mW cm^{-2}).

Donor	Treatment	V_{oc} [V]	J_{sc} [mA cm^{-2}]	FF	PCE [%]
DPPCC	n/a	0.84	3.30	0.29	0.82
	SVA	0.72	1.20	0.30	0.26
DPPBN-o	n/a	1.01	1.11	0.27	0.31
	SVA	0.66	0.09	0.31	0.02
DPPBN-i	n/a	0.75	3.10	0.30	0.70
	SVA	0.89	4.77	0.37	1.59

possibly due to different bulk-heterojunction morphologies. After exposure to CB vapor, the PCEs of the solar cells based on DPPCC and DPPBN-o dropped drastically to 0.26 and 0.02%, respectively. In contrast, the PCE of the DPPBN-i-based cell increased to 1.59%. These differences are mainly caused by the changes in J_{sc}, although V_{oc} and FF are also affected. For DPPCC and DPPBN-o, J_{sc} dropped from 3.30 and 1.11 mA cm^{-2} to 1.20 and 0.02 mA cm^{-2}, respectively, whereas the DPPBN-i-based device showed an increase in J_{sc} from 3.10 to 4.77 mA cm^{-2}. These changes in J_{sc} are reflected in the external quantum efficiency (EQE) spectra. After SVA, the EQE value decreased from 23.5 to 9.8% at 590 nm for DPPCC and from 7.24% to almost zero for DPPBN-o, whereas the EQE of DPPBN-i increased from 18.8 to 36.7% (Figure 5b). In particular, DPPCC has a maximum EQE corresponding to the 0–1 vibronic peak at 594 nm, whereas the EQE spectrum of DPPBN-i shows almost equivalent maxima corresponding to the 0–0 and 0–1 vibronic peaks at 660 and 605 nm, respectively. The EQE profiles of DPPCC and DPPBN-i are consistent with their optical absorption spectra, which indicate that the aggregation is similar in pure films and in blends with [60]PCBM. For the DPPBN-o-based solar cells the absorption also matches the EQE before SVA, but after annealing the response is virtually zero.

The device metrics listed in Table 5 suggest that the devices exhibit reasonable V_{oc} values, but a common limitation of these solar cells is their low J_{sc} (<5 mA cm^{-2}) and FF (<0.4). Hence, the charge-transport properties and bimolecular charge recombination losses were investigated. Hole mobilities μ_h were estimated from hole-only ITO/PEDOT:PSS/DPP:[60]PCBM/MoO_3/Ag devices after CB SVA by fitting the *J–V* data to a space-charge-limited current model, which resulted in a μ_h value of about 10^{-5} cm^{2}V^{-1}s^{-1} for all three donors (Figure 5c). The small μ_h values of the DPP:[60]PCBM films are likely responsible for the low FF. The hole mobilities of the blends decrease in the sequence DPPCC (3.6×10^{-5} cm^{2}V^{-1}s^{-1}) > DPPBN-i (1.8×10^{-5} cm^{2}V^{-1}s^{-1}) > DPPBN-o (7.0×10^{-6} cm^{2}V^{-1}s^{-1}), which is in accordance with the type of aggregation. For H-aggregation, the face-to-face stacking of the molecules offers a large area of π overlap among adjacent molecules, which results in higher hole mobility, the predominately J-aggregated DPPBN-o has the lowest hole mobility, and the predominately J-aggregated DPPBN-o the lowest hole mobility.

The dependence of J_{sc} on light intensity P_{light} was measured to investigate bimolecular recombination losses of the devices on CB SVA (Figure 5d). The J_{sc} of OSCs often shows a power-law dependence on the light intensity ($J_{sc} \sim P_{light}^{\alpha}$). The power-law component α is unity if bimolecular recombination losses are negligible.[24] The considerable deviation of the α values of the solar cells from unity (Figure 5d) indicates pronounced bimolecular recombination losses. SVA further decreases the α values for the blends with DPPCC and DPPBN-i, but leads to an increase in α for the DPPBN-i:[60]PCBM blend.

Morphology of DPP:[60]PCBM blends

The morphology of the blended films plays a key role in exciton diffusion, exciton dissociation, and charge transport, which determine the performance of bulk-heterojunction solar cells.[25] The morphology was investigated by AFM and TEM. The AFM measurements (Figure 6) showed that the films of DPP derivatives blended with [60]PCBM without SVA were smooth and uniform with similar and small root-mean square (RMS) surface roughness of 0.49, 0.46, and 0.43 nm, respectively. After SVA, the RMS roughness of the blended films increased considerably to 3.55, 3.93, and 3.09 nm, respectively, and this suggests that the domain sizes become larger as a consequence of crystallization.

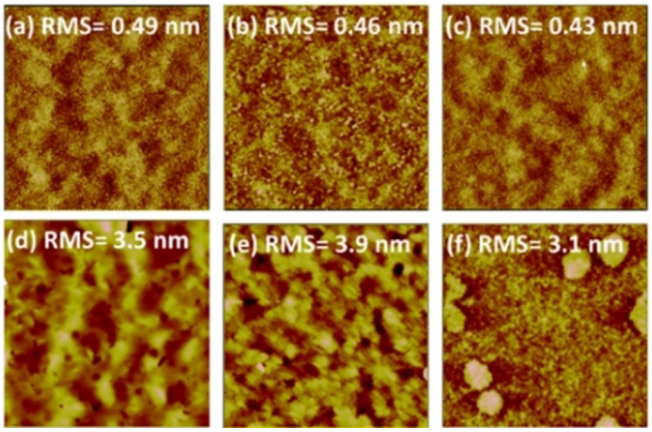

Figure 6. AFM height images for as-cast (a–c) and annealed (d–f) blends of a), d) DPPCC:[60]PCBM, b, e) DPPBN-o:[60]PCBM, and c, f) DPPBN-i:[60]PCBM. Image size: 5×5 μm.

The TEM images show that as-cast blend films of DPPCC and DPPBN-i are very uniform and lack detectable phase separation (Figure 7). Such intimately mixed morphologies are not beneficial to charge transport and can lead to severe geminate recombination. The blended film of DPPBN-o shows phase separation, which suggests that other factors also cause the poor device performance of DPPBN-o:[60]PCBM. After SVA, the blended films with DPPCC and DPPBN-o form very large domains that are detrimental to efficient charge transfer. The blended film of DPPBN-i exhibits improved phase separation with fibrillary structures after SVA, which is helpful for efficient charge generation and transport. The morphologies thus explain why the DPPBN-i:[60]PCBM blended film offers the highest PCE among the solar cell devices. Moreover, the combination of the hole mobility, the bimolecular recombination, and

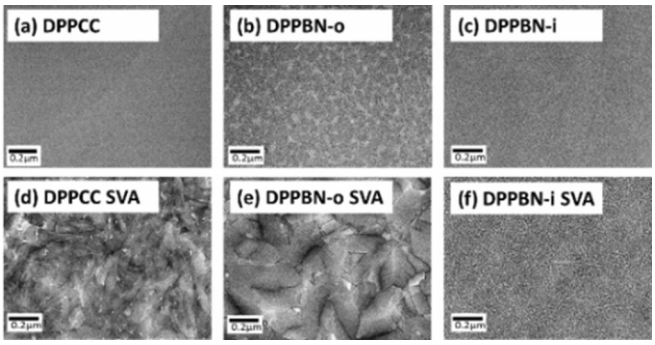

Figure 7. TEM images of as-cast (a–c) and solvent-annealed (d–f) blends: a), d) DPPCC:[60]PCBM, b, e) DPPBN-o:[60]PCBM, and c, f) DPPBN-i:[60]PCBM. Scale bar: 200 nm.

the morphology rationalizes the moderate photovoltaic performance of the DPP compounds in blends with [60]PCBM.

Photophysical properties of DPP:[60]PCBM blends

The photoluminescence spectra and lifetimes of the thin films of DPPs blended with [60]PCBM were measured to investigate the charge-transfer processes. The photoluminescence emission of the DPPs is considerably quenched after blending with [60]PCBM as a consequence of exciton dissociation at the interface between the donor and the acceptor (Figure S4, Supporting Information). This quenching is particularly stronger for DPPCC. Despite the strong quenching, the averaged fluorescence lifetimes of the blends of DPPBN-o and DPPBN-i with [60]PCBM are larger than those of the pure compounds (Table 3 and Figure S2 in the Supporting Information). Hence, the luminescence is likely due to residual photoluminescence from [60]PCBM ($\approx$700–800 nm) and cannot be used to determine the kinetics of the charge-transfer processes.

We also studied the PIA of the DPP derivatives in blends with [60]PCBM at 77 K (Figure 8). Although the PIA spectra in films are different from those in solution, the overall appearance and several of salient features are similar. The strongest peak is found at 1.74 ± 0.01 eV. This band is redshifted relative to the same band in toluene solution (1.83 ± 0.02 eV), which we attribute to the $T_1 \rightarrow T_n$ absorption. A second, less intense peak is found at about 1.2 eV. The nature of this peak can be either a lower-energy $T_1 \rightarrow T_n$ absorption or a signature of long-lived charges.

By adding quenchers with known triplet energy to the DPP:[60]PCBM mixtures, we can learn more about the nature of these excitations. If the triplet energy of the DPP derivatives is lower than the triplet energy of the quencher, the spectrum will not be affected. However, if the triplet energy of the quencher is lower than that of the DPP compound, the DPP triplet is quenched, and the triplet absorption of the quencher is observed. We used rubrene ($E(T_1) = 1.14$ eV) and bis(trihexylsiloxy)silicon 2,3-naphthalocyanine (SiNc, $E(T_1) = 0.93$ eV) to assess the triplet energies.[26,27] Figure 8 clearly shows that adding rubrene has no significant effect on the PIA spectra, but that SiNc quenches the entire spectrum and gives rise to the bleaching band of SiNc at 1.56 eV. This supports the view that the PIA spectra of the DPP:[60]PCBM blends are dominated by excitations in the triplet manifold. The quenching of the DPP triplet states by SiNc, but not by rubrene, places the triplet energy of the DPPs between 0.93 and 1.14 eV, roughly in agreement with the triplet energies obtained from the DFT calculations (Table 4). The absence of clear signatures of long-lived charges and the presence of DPP triplet states in the blended films suggest that the charge-separated states can recombine to the lower-lying triplet states on the DPP molecules in these blends. We note that the alternative explanation that the triplet states of DPP are formed by singlet fission, that is, $DPP(S_1) + DPP(S_0) \rightarrow 2\,DPP(T_1)$, is energetically possible because $E(S_1) > 2E(T_1)$ (Table 4), but does not occur (or does not result in long-lived T_1 states) because direct excitation of the DPP films did not give detectable triplet signals in the PIA spectrum.

Conclusions

Introducing B←N bonds to replace C–C bonds and changing the B←N bond orientation provides a means to change the crystallization behavior, aggregation, energy levels, and solar-cell performance of π-conjugated compounds. Substitution of C–C units by B←N units does not significantly affect the planarity of the molecules and has minor effect on the redox potentials or the optical absorption in solution. However, optical absorption and fluorescence spectra as well as excited-state

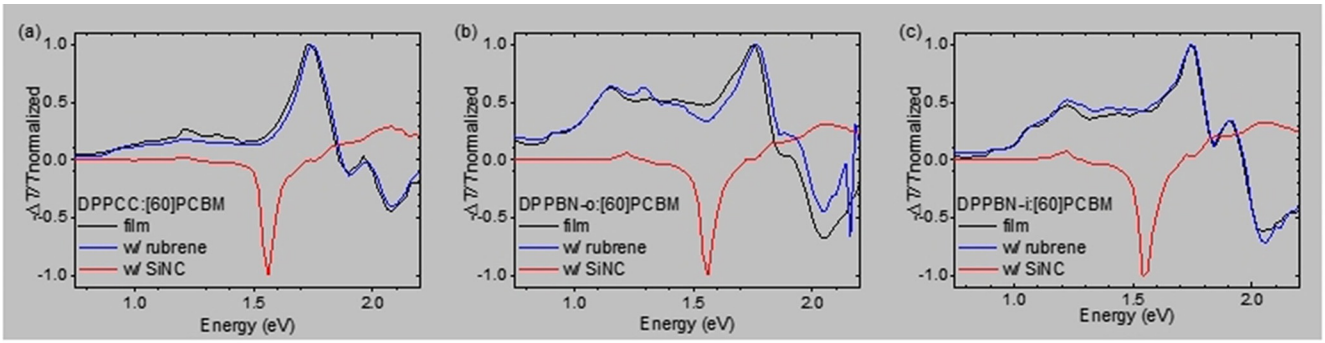

Figure 8. Normalized near-steady-state PIA spectra of spin-coated DPP:[60]PCBM (1:4 w/w) thin films without quencher (film) and with (w/) rubrene or SiNc as triplet quencher. In the latter case the DPP:[60]PCBM:quencher ratio was 1:4:1 (w/w/w). PIA spectra were recorded at 77 K, $\lambda_{exc} = 496$ or 514 nm. a) DPPCC. b) DPPBN-o. c) DPPBN-i.

lifetime measurements indicate that after thermal and SV annealing DPPCC forms H-aggregates in thin films, whereas DPPBN-o and DPPBN-i form J-aggregates. Photovoltaic devices with the three DPP compounds as donor and [60]PCBM as acceptor perform poorly. The best device, with PCE = 1.59%, was obtained for DPPBN-i after SVA. The devices exhibit similar V_{oc} values and hole mobilities, but bimolecular recombination and morphology limit the FF and thus the PCE.

Experimental Section

All experimental details are given in the Supporting Information.

Acknowledgements

The research was financially supported by the Recruitment Program of Global Youth Experts of China. This work was also supported by the Ministry of Science and Technology (Nos. 2017YFA0206600, 2014CB643501), and the Natural Science Foundation of China (Nos. 21520102006 and 91633301). M.M.-M. gratefully acknowledges the "Fundación Séneca, Agencia de Ciencia *y* Tecnología de la Región de Murcia" for a postdoctoral fellowship. The research has further received funding from the European Research Council under the European Union's Seventh Framework Programme (FP/2007-2013)/ERC Grant Agreement No. 339031 and from the Ministry of Education, Culture and Science (Gravity program 024.001.035).

Conflict of interest

The authors declare no conflict of interest.

Keywords: aggregation · B–N bonds · photovoltaic properties · semiconductors · thin films

[1] a) G. Yu, J. Gao, J. C. Hummelen, F. Wudl, A. J. Heeger, *Science* **1995**, *270*, 1789; b) R. Søndergaard, M. Hösel, D. Angmo, T. T. Larsen-Olsen, F. C. Krebs, *Mater. Today* **2012**, *15*, 36; c) L. Lu, T. Zheng, Q. Wu, A. M. Schneider, D. Zhao, L. Yu, *Chem. Rev.* **2015**, *115*, 12666.

[2] a) X. Che, Y. Li, Y. Qu, S. R. Forrest, *Nat. Energy* **2018**, *3*, 422; b) S. Zhang, Y. Qin, J. Zhu, J. Hou, *Adv. Mater.* **2018**, *30*, 1800868; c) S. Li, L. Ye, W. Zhao, H. Yan, B. Yang, D. Liu, W. Li, H. Ade, J. Hou, *J. Am. Chem. Soc.* **2018**, *140*, 7159; d) Y. Zhang, B. Kan, Y. Sun, Y. Wang, R. Xia, X. Ke, Y.-Q.-Q. Yi, C. Li, H.-L. Yip, X. Wan, Y. Cao, Y. Chen, *Adv. Mater.* **2018**, *30*, 1707508; e) H. Zhang, H. Yao, J. Hou, J. Zhu, J. Zhang, W. Li, R. Yu, B. Gao, S. Zhang, J. Hou, *Adv. Mater.* **2018**, *30*, 1800613; f) H. Li, Z. Xiao, L. Ding, J. Wang, *Sci. Bull.* **2018**, *63*, 340; g) Z. Xiao, X. Jia, L. Ding, *Sci. Bull.* **2017**, *62*, 1562; h) Y. F. Li, *Acta Phys.-Chim. Sin.* **2017**, *33*, 447; i) X. Zhang, *Acta Polym. Sin.* **2018**, *2*, 129.

[3] a) G. Zhang, J. Zhao, P. C. Y. Chow, K. Jiang, J. Zhang, Z. Zhu, J. Zhang, F. Huang, H. Yan, *Chem. Rev.* **2018**, *118*, 3447; b) C. Yan, S. Barlow, Z. Wang, H. Yan, A. K.-Y. Jen, S. R. Marder, X. Zhan, *Nat. Rev. Mater.* **2018**, *3*, 18003; c) J. Hou, O. Inganäs, R. H. Friend, F. Gao, *Nat. Mater.* **2018**, *17*, 119; d) C. Duan, F. Huang, Y. Cao, *J. Mater. Chem.* **2012**, *22*, 10416; e) C. Duan, F. Huang, Y. Cao, *Polym. Chem.* **2015**, *6*, 8081; f) J. You, L. Dou, K. Yoshimura, T. Kato, K. Ohya, T. Moriarty, K. Emery, C.-C. Chen, J. Gao, G. Li, Y. Yang, *Nat. Commun.* **2013**, *4*, 1446; g) C. H. Duan, K. Gao, F. J. M. Colberts, F. Liu, S. C. J. Meskers, M. M. Wienk, R. A. J. Janssen, *Adv. Energy Mater.* **2017**, *7*, 1700519; h) Z. H. Wu, Y. X. Zhu, W. Li, Y. P. Huang, J. W. Chen, C. H. Duan, F. Huang, Y. Cao, *Sci. China Chem.* **2016**, *59*, 1583; i) C. H. Duan, K. Gao, J. J. van Franeker, F. Liu, M. M. Wienk, R. A. J. Janssen, *J. Am. Chem. Soc.* **2016**, *138*, 10782.

[4] a) C. B. Nielsen, S. Holliday, H.-Y. Chen, S. J. Cryer, I. McCulloch, *Acc. Chem. Res.* **2015**, *48*, 2803; b) P. Cheng, G. Li, X. Zhan, Y. Yang, *Nat. Photonics* **2018**, *12*, 131; c) Y. Chen, X. Wan, G. Long, *Acc. Chem. Res.* **2013**, *46*, 2645; d) J. E. Coughlin, Z. B. Henson, G. C. Welch, G. C. Bazan, *Acc. Chem. Res.* **2014**, *47*, 257.

[5] a) Q. Li, Z. Li, *Adv. Sci.* **2017**, *4*, 1600484; b) C. Duan, G. Zango, M. G. Iglesias, F. J. M. Colberts, M. M. Wienk, M. V. Martínez-Díaz, R. A. J. Janssen, T. Torres, *Angew. Chem. Int. Ed.* **2017**, *56*, 148; *Angew. Chem.* **2017**, *129*, 154; c) C. Duan, D. Guzmán, F. J. M. Colberts, R. A. J. Janssen, T. Torres, *Chem. Eur. J.* **2018**, *24*, 6339; d) X. Liu, B. M. Xie, C. H. Duan, Z. J. Wang, B. B. Fan, K. Zhang, B. J. Lin, F. J. M. Colberts, W. Ma, *J. Mater. Chem. A* **2018**, *6*, 395; e) J. C. Jia, N. N. Zheng, Z. F. Wang, Y. P. Huang, C. H. Duan, F. Huang, Y. Cao, *Sci. China Chem.* **2017**, *60*, 1458.

[6] a) Q. Zhao, J. Liu, H. Wang, M. Li, K. Zhou, H. Yang, Y. Han, *J. Mater. Chem. C* **2015**, *3*, 8183; b) S. Mukherjee, C. M. Proctor, J. R. Tumbleston, G. C. Bazan, T.-Q. Nguyen, H. Ade, *Adv. Mater.* **2015**, *27*, 1105; c) L. Yang, S. Zhang, C. He, J. Zhang, Y. Yang, J. Zhu, Y. Cui, W. Zhao, H. Zhang, Y. Zhang, Z. Wei, J. Hou, *Chem. Mater.* **2018**, *30*, 2129; d) S. Li, L. Ye, W. Zhao, S. Zhang, H. Ade, J. Hou, *Adv. Energy Mater.* **2017**, *7*, 1700183; e) J. L. Wang, Z. F. Chang, X. X. Song, K. K. Liu, L. M. Jing, *J. Mater. Chem. C* **2015**, *3*, 9849.

[7] a) W. C. Lai, N. S. Dixit, R. A. Mackay, *J. Phys. Chem.* **1984**, *88*, 5364; b) K. Nakatsu, H. Yoshioka, S. Nishigaki, *J. Soc. Photogr. Sci. Technol. Jpn.* **1983**, *46*, 89.

[8] a) F. Würthner, T. E. Kaiser, C. R. Saha-Möller, *Angew. Chem. Int. Ed.* **2011**, *50*, 3376; *Angew. Chem.* **2011**, *123*, 3436; b) S. Ghosh, X.-Q. Li, V. Stepanenko, F. Würthner, *Chem. Eur. J.* **2008**, *14*, 11343; c) Y. Ren, A. M. Hiszpanski, L. Whittaker-Brooks, Y.-L. Loo, *ACS Appl. Mater. Interfaces* **2014**, *6*, 14533; d) F. Fennel, S. Wolter, Z. Xie, P.-A. Plötz, O. Kühn, F. Würthner, S. Lochbrunner, *J. Am. Chem. Soc.* **2013**, *135*, 18722; e) F. C. Spano, C. Silva, *Annu. Rev. Phy. Chem.* **2014**, *65*, 477.

[9] a) V. S. Gevaerts, E. M. Herzig, M. Kirkus, K. H. Hendriks, M. M. Wienk, J. Perlich, P. Müller-Buschbaum, R. A. J. Janssen, *Chem. Mater.* **2014**, *26*, 916; b) M. Más-Montoya, R. A. J. Janssen, *Adv. Funct. Mater.* **2017**, *27*, 1605779.

[10] a) W. Li, K. H. Hendriks, M. M. Wienk, R. A. J. Janssen, *Acc. Chem. Res.* **2016**, *49*, 78; b) Y. Li, P. Sonar, L. Murphy, W. Hong, *Energy Environ. Sci.* **2013**, *6*, 1684; c) C. B. Nielsen, M. Turbiez, I. McCulloch, *Adv. Mater.* **2013**, *25*, 1859.

[11] X.-Y. Wang, J.-Y. Wang, J. Pei, *Chem. Eur. J.* **2015**, *21*, 3528.

[12] a) D. Frath, J. Massue, G. Ulrich, R. Ziessel, *Angew. Chem. Int. Ed.* **2014**, *53*, 2290; *Angew. Chem.* **2014**, *126*, 2322; b) X.-Y. Wang, H.-R. Lin, T. Lei, D.-C. Yang, F.-D. Zhuang, J.-Y. Wang, S.-C. Yuan, J. Pei, *Angew. Chem. Int. Ed.* **2013**, *52*, 3117; *Angew. Chem.* **2013**, *125*, 3199; c) N. Ishida, T. Moriya, T. Goya, M. Murakami, *J. Org. Chem.* **2010**, *75*, 8709; d) C. Dou, Z. Ding, Z. Zhang, Z. Xie, J. Liu, L. Wang, *Angew. Chem. Int. Ed.* **2015**, *54*, 3648; *Angew. Chem.* **2015**, *127*, 3719; e) C. Dou, X. Long, Z. Ding, Z. Xie, J. Liu, L. Wang, *Angew. Chem. Int. Ed.* **2016**, *55*, 1436; *Angew. Chem.* **2016**, *128*, 1458; f) Y. Min, C. Dou, H. Tian, Y. Geng, J. Liu, L. Wang, *Angew. Chem. Int. Ed.* **2018**, *57*, 2000; *Angew. Chem.* **2018**, *130*, 2018; g) J. Yu, D. Yu, Y. Chen, H. Chen, M.-Y. Lin, B.-M. Cheng, J. Li, W. Duan, *Chem. Phys. Lett.* **2009**, *476*, 240.

[13] a) L. R. Thorne, R. D. Suenram, F. J. Lovas, *J. Chem. Phys.* **1983**, *78*, 167; b) D. J. Grant, D. A. Dixon, *J. Phys. Chem. A* **2006**, *110*, 12955.

[14] a) W.-K. Chan, Y. Chen, Z. Peng, L. Yu, *J. Am. Chem. Soc.* **1993**, *115*, 11735; b) G. Lange, B. Tieke, *Macromol. Chem. Phys.* **1999**, *200*, 106.

[15] V. Parra, T. del Caño, M. J. Gómez-Escalonilla, F. Langa, M. L. Rodríguez-Méndez, J. A. De Saja, *Synth. Met.* **2005**, *148*, 47.

[16] P. G. Campbell, A. J. V. Marwitz, S.-Y. Liu, *Angew. Chem. Int. Ed.* **2012**, *51*, 6074; *Angew. Chem.* **2012**, *124*, 6178.

[17] J. Wang, S. Wang, C. Duan, F. J. M. Colberts, J. Mai, X. Liu, X. Jia, X. Lu, R. A. J. Janssen, F. Huang, Y. Cao, *Adv. Energy Mater.* **2017**, *7*, 1702033.

[18] M. C. Scharber, D. Mühlbacher, M. Koppe, P. Denk, C. Waldauf, A. J. Heeger, C. J. Brabec, *Adv. Mater.* **2006**, *18*, 789.

[19] C. M. Cardona, W. Li, A. E. Kaifer, D. Stockdale, G. C. Bazan, *Adv. Mater.* **2011**, *23*, 2367.

[20] M. Kasha, *Radiat. Res.* **1963**, *20*, 55.

[21] a) F. C. Spano, *Acc. Chem. Res.* **2010**, *43*, 429; b) N. J. Hestand, F. C. Spano, *Acc. Chem. Res.* **2017**, *50*, 341.
[22] B. P. Karsten, R. K. M. Bouwer, J. C. Hummelen, R. M. Williams, R. A. J. Janssen, *Photochem. Photobiol. Sci.* **2010**, *9*, 1055.
[23] S.-O. Kim, T. K. An, J. Chen, I. Kang, S. H. Kang, D. S. Chung, C. E. Park, Y.-H. Kim, S.-K. Kwon, *Adv. Funct. Mater.* **2011**, *21*, 1616.
[24] a) A. K. K. Kyaw, D. H. Wang, D. Wynands, J. Zhang, T.-Q. Nguyen, G. C. Bazan, A. J. Heeger, *Nano Lett.* **2013**, *13*, 3796; b) L. J. A. Koster, V. D. Mihailetchi, R. Ramaker, P. W. M. Blom, *Appl. Phys. Lett.* **2005**, *86*, 123509; c) M. M. Mandoc, F. B. Kooistra, J. C. Hummelen, B. de Boer, P. W. M. Blom, *Appl. Phys. Lett.* **2007**, *91*, 263505.
[25] a) L. Ye, H. Hu, M. Ghasemi, T. Wang, B. A. Collins, J.-H. Kim, K. Jiang, J. H. Carpenter, H. Li, Z. Li, T. McAfee, J. Zhao, X. Chen, J. L. Y. Lai, T. Ma, J.-L. Brédas, H. Yan, H. Ade, *Nat. Mater.* **2018**, *17*, 253; b) Y. Huang, E. J. Kramer, A. J. Heeger, G. C. Bazan, *Chem. Rev.* **2014**, *114*, 7006; c) F. Liu, C. Wang, J. K. Baral, L. Zhang, J. J. Watkins, A. L. Briseno, T. P. Russell, *J. Am. Chem. Soc.* **2013**, *135*, 19248; d) S. D. Collins, N. A. Ran, M. C. Heiber, T.-Q. Nguyen, *Adv. Energy Mater.* **2017**, *7*, 1602242.
[26] W. G. Herkstroeter, P. B. Merkel, *J. Photochem.* **1981**, *16*, 331.
[27] P. A. Firey, W. E. Ford, J. R. Sounik, M. E. Kenney, M. A. J. Rodgers, *J. Am. Chem. Soc.* **1988**, *110*, 7626.

Manuscript received: August 6, 2018
Revised manuscript received: October 1, 2018
Accepted manuscript online: October 4, 2018
Version of record online: December 10, 2018

